Low temperature short-range ordering caused by Mn^{2+} doping of $Rb_3H(SO_4)_2$

2010 J. Phys.: Condens. Matter 22 225901

(http://iopscience.iop.org/0953-8984/22/22/225901)

J. Phys.: Condens. Matter **22** (2010) 225901 (5pp) doi:10.1088/0953-8984/22/22/225901

Low temperature short-range ordering caused by Mn^{2+} doping of $Rb_3H(SO_4)_2$

W Bednarski, A Ostrowski and S Waplak

Institute of Molecular Physics, Polish Academy of Sciences, M. Smoluchowskiego 17, 60-179 Poznań, Poland

Received 5 March 2010, in final form 20 April 2010
Published 12 May 2010
Online at stacks.iop.org/JPhysCM/22/225901

Abstract

The low temperature behaviour of $Rb_3H(SO_4)_2$ and $Rb_3D(SO_4)_2$ and their doped analogues was investigated by means of their dielectric response. Electron paramagnetic resonance was used to control the impurity concentration. Influence of different admixtures on ferroic properties is discussed. It has been shown that an appropriately chosen impurity in doped $Rb_3H(SO_4)_2$ can lead to a short-range ordering similar to that observed for doped incipient ferroelectric-like $SrTiO_3$ and $KTaO_3$.

1. Introduction

The hydrogen-bonded crystals of the $Me_3A(XO_4)_2$ family (Me = K, Rb, Tl, NH_4, Cs; A = H, D; X = S, Se) are of great interest due to superionic properties at high temperature [1–6] and an unusually large isotopic effect clearly observed at low temperatures [7–9]. In contrast to $(NH_4)_3A(XO_4)_2$, most crystals of the $Me_3A(XO_4)_2$ group have rather simple phase diagrams revealing only one or two phase transitions at low temperatures. Some crystals undergo a low temperature ferroic phase transition when deuterated, even in part, but do not show it in the protonated form (complete H/D isotope effect) [8]. In the latter case, the electric permittivity at low temperatures becomes almost temperature-independent. The absence of a phase transition is usually ascribed to quantum fluctuations of atoms that suppress the phase transition in the quantum paraelectric state of the protonated crystals. The critical temperature T_c of the antiferroelectric phase transition depends on the H/D content ratio and increases with the increasing deuterium ion concentration [8]. This behaviour has essentially been elucidated theoretically by applying the transverse Ising model [9] or a model where the proton potential is strongly affected by a low-frequency heavy-atom mode [10]. In the latter model the proton couples strongly to the dipole produced by a local vibration mode of the dimer comprising two neighbouring SO_4 tetrahedra. The latter mode is due to the dipole–dipole interaction between two neighbouring dimers [10]. Finally, the proton does not reside in a well-defined single-particle potential, but rather in a potential that is strongly affected by a local vibrational mode [11]. This model is consistent with the experimental values of the critical temperature T_c depending on the hydrogen bond lengths in the family of $Me_3A(XO_4)_2$ crystals. A similar isotopic effect was observed for quantum paraelectric $SrTiO_3$ crystals, wherein a ferroelectric state was induced by a $^{16}O/^{18}O$ substitution [12]. Quantitative analyses performed in [12] for ferroelectric $SrTi(^{16}O_{1-x}{}^{18}O_x)_3$ ($x \geqslant 0.33$) showed that the replacement of ^{16}O with ^{18}O suppresses the quantum fluctuations in $SrTiO_3$ and leaves the ferroelectric fluctuation almost unchanged. $KTaO_3$ represents another interesting example of a quantum paraelectric intensively studied in the last decades. It has been shown that, for Li-doped $KTaO_3$, above the critical concentration $x = 0.022$, $K_{1-x}Li_xTaO_3$ undergoes a first-order ferroelectric phase transition and that below $x = 0.022$ it remains in a polar glass state [13–15].

Our previous studies revealed a significant influence of a small amount of Mn^{2+} ions on the electric transport properties and on the temperature of the superionic phase transition in $Me_3H(SO_4)_2$ compounds [2, 3]. An anomalous temperature dependence of the EPR parameters of $Rb_3H(SO_4)_2$:Mn^{2+} was observed [16] close to the temperature of the antiferroelectric phase transition of $Rb_3D(SO_4)_2$ (abbreviated as RDS). However, recent results concerning the dielectric properties confirmed that there are no phase transitions at this or lower temperatures down to 30 K for the Mn^{2+}-doped $Rb_3H(SO_4)_2$ (abbreviated as RHS) compound [3].

The main aim of the present work is the verification of the hypothesis that small amounts of various admixtures in $Rb_3H(SO_4)_2$ cause similar effects to those observed in other quantum paraelectrics close to liquid helium temperature. This paper also provides an explanation of the differences between the antiferroelectric phase transition temperature values in $Rb_3D(SO_4)_2$ quoted by other authors [8, 10, 17, 18].

Table 1. Concentration of various impurities in doped RHS/RDS single crystals and in solutions.

Crystal	10^6 × number of Cr^{6+}, VO^{2+} or Mn^{2+} ions/number of $1/3Rb^+$ or S^{6+} ions in solution (ppm)	10^6 × number of Cr^{6+}, VO^{2+} or Mn^{2+} ions/number of $1/3Rb^+$ or S^{6+} ions in crystal (ppm)
$Rb_3H(SO)_4:Cr^{6+}$	12 200 (50)	12 200 (50)[a]
$Rb_3H(SO)_4:VO^{2+}$	15 300 (50)	860 (90)
$Rb_3H(SO)_4:Mn^{2+}$	17 400 (50)	10 000 (1000)
$Rb_3D(SO)_4:Mn^{2+}$ [b]	17 400 (50)	16 000 (1600)
$Rb_3D(SO)_4:Mn^{2+}$ [c]	17 400 (50)	15 000 (1500)

[a] Concentration of Cr^{6+} ions in $Rb_3H(SO_4)_2:Cr^{6+}$ single crystals estimated from the $Cr^{6+}/(Cr^{6+} + S^{6+})$ ratio in the solution.
[b] Crystal prepared from the solution kept in a dry nitrogen atmosphere.
[c] Crystal prepared from the solution kept in air.

2. Experimental details

Pure $Rb_3A(SO_4)_2$ (A = H or D) crystals were prepared at room temperature (RT) by slow evaporation of solutions containing 1.66 g Rb_2SO_4 + 0.15 ml H_2SO_4 + H_2O or 1.66 g Rb_2SO_4 + 0.15 ml D_2SO_4 + D_2O for protonated and deuterated compounds, respectively. $Rb_3A(SO_4)_2$ crystals doped with Mn^{2+} impurities were obtained by adding 0.016 g of $MnSO_4{\cdot}4H_2O$ to these solutions. Deuterated crystals, except the one quoted hereafter, were grown from the solutions kept in a dry nitrogen atmosphere to avoid H_2O condensation from air. Due to the use of $MnSO_4{\cdot}4H_2O$, the concentration of protons in RDS:Mn^{2+} crystals amounted to about 1600 ppm. For comparison, $Rb_3D(SO_4)_2:Mn^{2+}$ grown from an initially fully deuterated solution kept in air has also been prepared. RHS:VO^{2+} and RHS:Cr^{6+} were prepared from fully protonated solutions containing an additional 0.016 g of $VOSO_4{\cdot}5H_2O$ or $K_2Cr_2O_7$, respectively.

X-band EPR measurements were performed with a Bruker ELEXSYS X-band spectrometer. The EPR spectra were recorded at RT as derivatives of the microwave absorption. In order to determine the concentration of paramagnetic impurities in the samples, the spectra were double-integrated and compared with the standard intensity of an $Al_2O_3:Cr^{3+}$ single crystal with a known spin concentration. Silver paste electrodes were deposited on the (100) plane at RT and served for dielectric studies. The complex electric permittivity ε of the samples was measured in the frequency range of 1 kHz–1 MHz with an HP4284A LCR meter in the temperature range of 4.2–295 K. The temperature was controlled and stabilized with a LakeShore 340 temperature controller.

3. Results

Table 1 gives the concentration of impurities in the crystals and solutions. There are two sets of rubidium ions and one type of SO_4^{2-} ions in the RHS crystal structure at room temperature. Each $Rb_3H(SO_4)_2$ formula consists of one Rb^+(I)-type ion in a special position on the twofold axis and two Rb^+(II)-type ions positioned differently (see [3], figure 2 therein). The

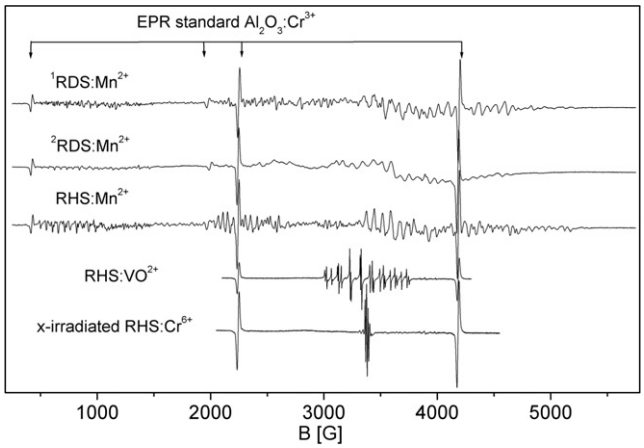

Figure 1. EPR spectra of $Rb_3A(SO_4)_2$ single crystals doped with various paramagnetic centres recorded in an external magnetic field parallel to the (100) direction. Positions of the lines of the standard (recorded in the opposite phase) are marked by arrows. [1]—crystal prepared from the solution kept in dry nitrogen atmosphere, [2]—crystal prepared from the solution kept in air.

Mn^{2+} as well as VO^{2+} ions replace only the Rb^+(I)-type ions in the crystal structure and the resulting excess charge is compensated by proton vacancies [3, 19]. This is why the concentrations of Mn^{2+} and VO^{2+} were calculated per $Rb_3H(SO_4)_2$ formula unit and that of Cr^{6+} per SO_4^{2-} ion. The data for the crystals, except RHS:Cr^{6+}, were obtained following the EPR spectra double-integration procedure. Some examples of the EPR spectra recorded for the samples studied are presented in figure 1. One should notice a large difference between the concentrations of the Mn^{2+} and VO^{2+} impurities in the crystals in spite of comparable concentrations in the solutions. The higher concentration of the Mn^{2+} ions can result from their smaller ionic radii of 0.97 Å in comparison with that (1.67 Å) of the VO^{2+} ions [20, 21].

The Cr^{6+} content in RHS: Cr^{6+} crystals (Cr^{6+} is not a paramagnetic ion) was estimated from the $Cr^{6+}/(Cr^{6+} + S^{6+})$ ratio in the solution by assuming that a chromium ion can be doped to the crystal structure with the same probability as a sulfur one. This approach appears to be justified because CrO_4^{2-} replaces the SO_4^{2-} group and, unlike the VO^{2+} or Mn^{2+} ions, needs no charge compensation. After an x-ray irradiation of RHS:Cr^{6+} (for 5 h with the x-ray generated in a cobalt valve source operating at 30 kV and 20 mA), the EPR spectra consist of SO_4^- and CrO_4^{3-} lines and confirm the incorporation of the CrO_4 groups into the crystal lattice. The integral intensity of the EPR spectrum for x-ray-irradiated RHS:Cr^{6+} is lower than expected from the estimation presented in table 1 and results from only a partial conversion (a few %) of the non-paramagnetic CrO_4^{2-} ions into the paramagnetic CrO_4^{3-} ones in the irradiation process: $SO_4^{2-} + CrO_4^{2-} \overset{x-ray}{\rightarrow} SO_4^- + CrO_4^{3-}$.

Figure 2 presents the temperature dependence of the electric permittivity measured for pure and Mn^{2+}-doped RHS and RDS single crystals. The RDS samples prepared from the solution kept in dry nitrogen atmosphere during the crystal growth reveal an antiferroelectric phase transition at T_c = 86.5 K. Let us notice that the value of T_c measured

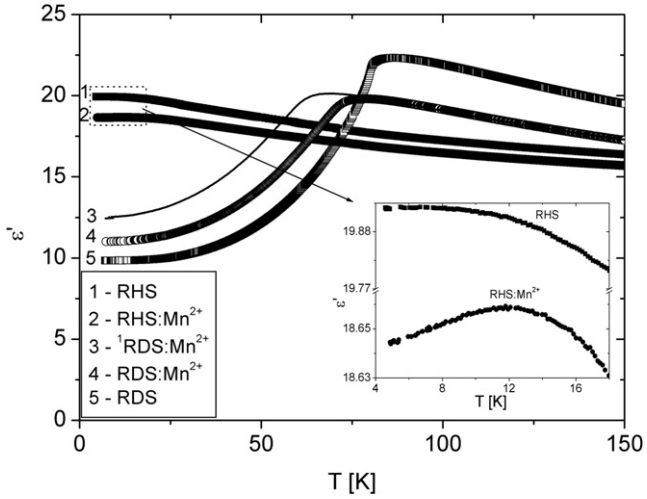

Figure 2. The real part of the electric permittivity ε' measured at $f = 10$ kHz for pure and Mn^{2+}-doped RHS and RDS single crystals as a function of temperature. [1]—thin solid line represents the dielectric data obtained for $Rb_3D(SO_4)_2$:Mn^{2+} grown from deuterated solution kept in air. The inset presents the low temperature range of the electric permittivity ε' for RHS and RHS:Mn^{2+} crystals.

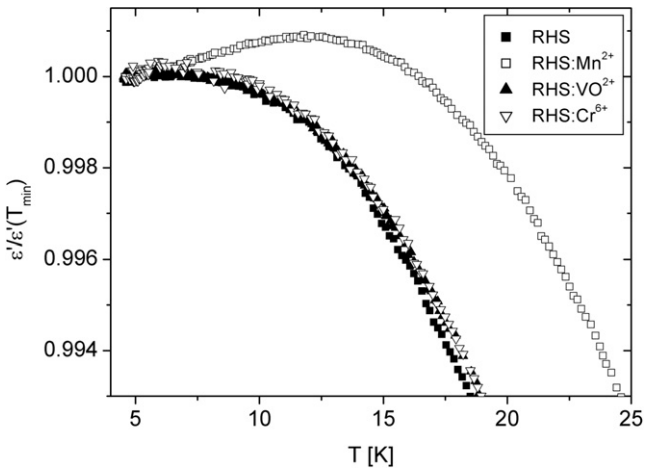

Figure 3. The real part of the electric permittivity ε' as a function of temperature, measured at $f = 10$ kHz and normalized to its value $\varepsilon'(T_{min})$ at the lowest measured temperatures T_{min} for pure RHS crystals and those doped with different impurities.

by us is at least a few Kelvin higher than those reported earlier [8, 10, 17, 18]. This testifies to the good quality of our crystals. In particular, the dry nitrogen atmosphere prevented the introduction of the condensed H_2O molecules into the solution from air as well as the incorporation of protons into the crystal structure.

Obviously, the Mn^{2+} impurity partially destroys the antiferroelectric ordering since the phase transition temperature T_c decreases to 78.6 and 69.0 K for the grown-in-nitrogen atmosphere and grown-in-air RDS:Mn^{2+}, respectively (see lines 3 and 4 in figure 2). The lower T_c value of 69 K (see line 3 in figure 2) corresponds to the compound grown from the deuterated solution kept in air. This is the evidence for the introduction

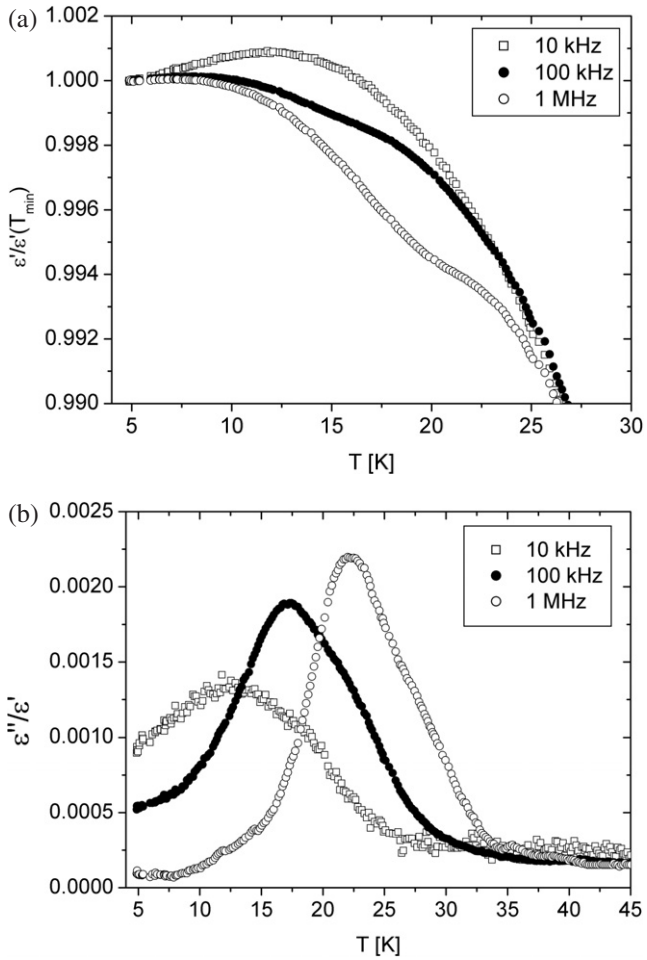

Figure 4. (a) The real part of the electric permittivity ε' normalized to that $\varepsilon'(T_{min})$ at the lowest measured temperature T_{min} and (b) the ratio $\varepsilon''/\varepsilon'$ of the imaginary and real parts of the electric permittivity for RHS:Mn^{2+} measured at several frequencies as a function of temperature.

of condensed H_2O into the initially fully deuterated solution, leading to the incorporation of protons into the RDS:Mn^{2+}.

In contrast to the case of the pure protonated crystals, the real part of the electric permittivity ε' of the RHS:Mn^{2+} reveals a weak maximum at low temperature. As seen in figure 3, no maxima can be observed for RHS doped by impurities other than Mn^{2+}. Precise measurements of the electric permittivity for RHS:Mn^{2+} demonstrate not only a low temperature dispersion (figure 4(a)) but also characteristic frequency-dependent maxima in the $\varepsilon''/\varepsilon'$ ratio (figure 4(b)) plotted as a function of temperature. These anomalies will be discussed hereafter.

4. Discussion

It has been shown in [22] that the dielectric response versus temperature in a mixed ferroglass phase reveals frequency-dependent maxima. The position T_m of a maximum in the temperature scale can be analysed with the help of the formula:

$$T_m(\omega) = T_g - \frac{V}{\ln(\omega\tau_0)}, \qquad (1)$$

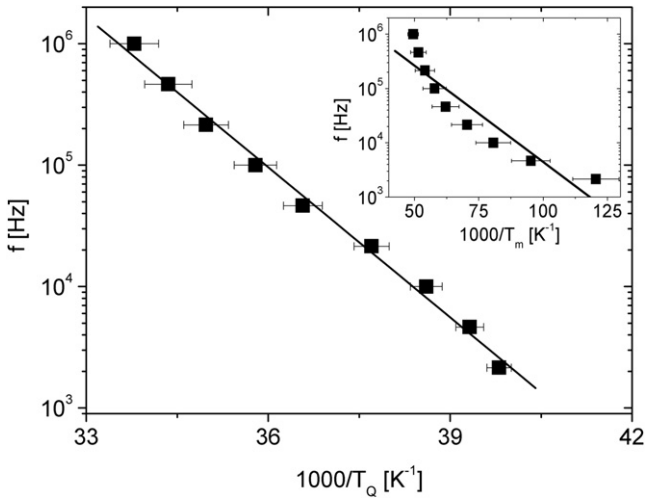

Figure 5. The frequency f of the $\varepsilon''/\varepsilon'$ versus T maxima shown in part in figure 4(b), plotted in an inverse quantum temperature scale as a function of $1000/T_Q$. The values of the quantum temperature $T_Q = T_Q(T_m)$ were calculated with the help of equation (2) from the values of temperatures T_m at which the $\varepsilon''/\varepsilon'$ maxima have been noticed. The inset demonstrates that the classical Arrhenius law is not fulfilled.

where τ_0 and V are the pre-exponential factor and the barrier height in the expression for the temperature dependence of the relaxor relaxation time, respectively. The choice of the T_g value leads either to the Arrhenius law ($T_g = 0$) or to the Vogel–Fulcher law ($T_g > 0$). It is obvious from the inset presented in figure 5 that the classical Arrhenius law is not followed. An attempted similar fit of the data to the Vogel–Fulcher law, not shown here, also appears unsatisfactory. On the other hand, the real part of the electric permittivity of pure RHS crystals and those doped with Cr^{6+} or VO^{2+} ions behaves in a similar way as that observed in other quantum paraelectrics [23, 24]. Therefore, it seems desirable to apply a quantum-mechanical treatment [25, 26], in particular at low temperatures, to describe the dispersion of T_m values. In general, according to the concept of a quantum temperature, susceptibility of a ferroelectric system follows the Barrett law [25] rather than the classical Curie–Weiss law. The so-called quantum temperature scale QTS is defined by the equation proposed in [27]:

$$T_Q = T_S \coth \frac{T_S}{T}, \tag{2}$$

where T_Q is the quantum temperature and T_S is the saturation temperature related to the ground state energy of the quantum oscillator.

Figure 5 shows the Arrhenius law fulfilment by applying QTS to the experimental data obtained from measurements on RHS:Mn^{2+} single crystals (see figure 4(b)). The best approximation gives the following values of the parameters: $T_S = 25(2)$ K and $V = 82(3)$ meV. The latter energy value agrees well with the proton excitation energies in the double-well potential obtained from the inelastic neutron scattering spectra [28].

Table 2. Ionic radii of the impurities and the ions replaced by them after [20, 21].

Ion	Radius (Å)
Rb^+	1.66
S^{6+}	0.26
Mn^{2+}	0.97
VO^{2+}	1.67
Cr^{6+}	0.40

In order to understand the different behaviours of the dielectric response of the RHS:Mn^{2+} and RHS with other dopants, the comparison of the concentrations of the impurities and first of all their ionic radii presented in table 2 could be useful. It is obvious that changes induced by the impurities in their surroundings affect the ion attraction and repulsion forces as well as interactions between the unit cells. In particular, impurities can change the lengths of the hydrogen bonds responsible for ferroic properties. Longer hydrogen bonds are present in deuterated crystals. Among the impurities studied, only Mn^{2+} replaces Rb^+ with an ionic radius larger than its own [21]. This leads to an attraction of neighbouring SO_4^{2-} anions to the Mn^{2+} cation and to an elongation of the hydrogen bond in the $SO_4\cdots H–SO_4$ dimers. Thus, Mn^{2+} doping can give rise to an effect similar to deuteration, i.e. to the hydrogen bond ordering in the immediate neighbourhood of the impurity in RHS:Mn^{2+}. On the other hand, hydrogen bonds in RDS:Mn^{2+} have different lengths near to and far from Mn^{2+}, which results in weak cooperative interactions between the $SO_4\cdots D–SO_4$ dimers. One should have in mind that Mn^{2+} requires a charge compensation (proton and/or deuteron vacancy) which, in addition, disturbs the long-range order. Moreover, the distribution of impurities in the crystal structure should be inhomogeneous, because the ratio of dopants to substituted ions in the initial solution is different from that in the crystals studied. All the above effects lead to a decrease in the antiferroelectric phase transition temperature in RDS:Mn^{2+} crystals.

5. Conclusions

Frequency dependences of low temperature maxima for RHS:Mn^{2+} were described in a quantum temperature scale by the Arrhenius law with an activation energy of 82 meV. The Mn^{2+} admixture within $Rb_3H(SO_4)_2$:Mn^{2+} elongates the nearby hydrogen bond due to the difference in its ionic radius and charge with respect to the replaced Rb^+ ion. This leads to a short-range proton ordering in the double-well potential as indicated by the dispersion of the dielectric response. The lack of a similar dispersion at low temperature for other dopants like VO^{2+} and Cr^{6+} in $Rb_3H(SO_4)_2$ results from comparable ionic radii of the admixtures and the replaced ions in the latter case. Different hydrogen bond lengths near to and far from Mn^{2+} ions in the doped RDS lead to an antiferroelectric–paraelectric phase transition temperature lowering due to the weakness of the cooperative interactions between the $SO_4\cdots D–SO_4$ dimers.

References

[1] Pawłowski A and Połomska M 2005 *Solid State Ion.* **176** 2045
[2] Bednarski W, Ostrowski A and Waplak S 2008 *Solid State Ion.* **179** 1974
[3] Ostrowski A and Bednarski W 2009 *J. Phys.: Condens. Matter* **21** 205401
[4] Haile S M 2003 *Acta Mater.* **51** 5981
[5] Bednarski W and Waplak S 2006 *J. Phys. D: Appl. Phys.* **39** 4664
[6] Cowan L A, Morcos R M, Hatada N, Navrotsky A and Haile S M 2008 *Solid State Ion.* **179** 305
[7] Homouz D, Reiter G, Eckert J, Mayers J and Blinc R 2007 *Phys. Rev. Lett.* **98** 115502
[8] Gesi K 1992 *J. Phys. Soc. Japan* **61** 162
[9] Morimoto Y, Tokura Y, Nagaosa N, Suzuki T and Kumagai K 1993 *Phys. Rev. Lett.* **71** 2833
[10] Merunka D and Rakvin B 2009 *Phys. Rev.* B **79** 132108
[11] Ikeda S and Yamada Y 1995 *Physica* B **213/214** 652
[12] Wang R and Itoh M 2001 *Phys. Rev.* B **64** 174104
[13] Kleemann W, Kutz S and Rytz D 1987 *Europhys. Lett.* **4** 239
[14] Kleemann W, Kutz S, Schafer F J and Rytz D 1988 *Phys. Rev.* B **37** 5856
[15] Schremmer H, Kleemann W and Rytz D 1989 *Phys. Rev. Lett.* **62** 1896
[16] Bednarski W, Ostrowski A and Waplak S 2008 *Solid State Commun.* **146** 365
[17] Dolinšek J, Mikac U, Javoršek J E, Lahajnar G, Blinc R and Kirpichnikova L F 1998 *Phys. Rev.* B **58** 8445
[18] Titze A, Hinze G and Böhmer R 1998 *Phys. Rev.* B **57** R666
[19] Ostrowski A, Waplak S and Bednarski W 2005 *Acta Phys. Pol.* A **108** 127
[20] Ballhausen C J and Gray H B 1962 *Inorg. Chem.* **1** 111
[21] Shannon R D 1976 *Acta Crystallogr.* A **32** 751
[22] Glinchuk M D, Stephanovich V A, Hilczer B, Wolak J and Caranoni C 1999 *J. Phys.: Condens. Matter* **11** 6263
[23] Kleemann W, Dec J and Westwański B 1998 *Phys. Rev.* B **58** 8985
[24] Dec J and Kleemann W 1999 *J. Phys.: Condens. Matter* **11** L379
[25] Barrett J H 1952 *Phys. Rev.* **86** 118
[26] Salje E K H, Wruck B and Thomas H 1991 *Z. Phys.* B **82** 399
[27] Dec J and Kleemann W 1998 *Solid State Commun.* **106** 665
[28] Fillux F, Lautie A, Tomkinson J and Kearly G J 1991 *Chem. Phys.* **154** 135